

Short Communication

First Principles Design of Anthraquinone Derivatives in Redox Flow Batteries

Liangliang Chen¹, Chengwei Ma¹, Xin Li^{1,*}, Luyin Lin^{2,*}, Shengsian Yang², Ge Li¹

¹ School of Chemistry and Chemical Engineering, Beijing Institute of Technology, 100081, Beijing, China

² Department of Chemical Engineering and Biotechnology, National Taipei University of Technology (Taipei Tech), Taipei, 10608, Taiwan

*E-mail: klkxlx@163.com, lylin@mail.ntut.edu.tw

Liangliang Chen and Chengwei Ma contributed equally to this work.

Received: 20 July 2017 / Accepted: 5 September 2017 / Published: 12 October 2017

The redox flow battery (RFB), which is famous for its low cost and durability, could improve the utilization of renewable energy. We employed density functional calculations to calculate the intrinsic solubility of 9,10-anthraquinone derivatives and found that –OH groups could theoretically improve the solubility to exceed 5 mol L⁻¹. Moreover, the reduction potential was calculated for 9,10-anthraquinone derivatives with –OH substitutions at different positions. 1,8-dihydroxyanthraquinone was found to exhibit excellent electrochemical activity, as validated by electrochemical measurements. The diffusion coefficient and kinetic rate constant were faster than those of conventional materials. This is a comparatively integral work that uses first principles calculations to efficiently determine the organic redox flow of battery materials.

Keywords: Redox flow battery, First principles calculation, Solubility, Reduction potential, Anthraquinone derivatives

1. INTRODUCTION

Motivated by the depletion of oil reserves and the intensification of the greenhouse effect, the demand for renewable energy (such as wind energy and solar energy) has increased dramatically. As is known, these demands are affected by the surrounding environment and climate to a great extent. Therefore, use of such sources will be greatly limited without a matching energy storage capability. In addition, there is always a mismatch between energy supply and demand, resulting in a great waste of

energy. To overcome these limitations, one requires large-scale and effective energy storage devices to regulate energy storage and supply processes.[1-5]

Compared to the current battery technologies, redox flow batteries (RFBs) are safe, inexpensive and sustainable. The use of liquid redox-active species avoids the generation of mechanical strain during cycling, which can lead to an extended service life. Although all-vanadium RFBs have been widely deployed, vanadium has been difficult to prepare and is expensive, with a price as high as \$40 per kilogram, which limits its wide-scale application.[6-10]

Anthraquinone derivatives have been developed to replace vanadium as redox-active species in aqueous flow batteries because of their fast redox kinetics and chemical tenability. Compared to a non-aqueous flow battery, implementation of the aqueous flow battery presents relatively fewer engineering technical challenges and thus has commercial potential.[11-16]

For an aqueous flow battery, a wide redox window of its redox active materials as well as high solubility are required to improve its energy density.[17] Nevertheless, it can be difficult to obtain suitable materials for RFBs based only on experiments because numerous organic compounds with different functional group substitutions exist. Recently, researchers have found that it can be more efficient to predict the physical properties of candidate materials by first principles calculations, which could greatly improve the calculation efficiency. Guzik et al. have studied as many as 1710 quinone (Q) and hydroquinone (QH₂) redox couples, with various substituents, to look for promising candidates for RFBs.[18] Schrier et al. explored thiophenoquinones with different kinds of functional group substitutions and identified 1056 potential molecules within 10611 possible combinations.[19] Han et al. calculated 106 molecule candidates and found fluoro-methoxybenzotrile and dimethoxyoltafluorohiphenyl to be promising redox active materials for RFBs.[20] However, all of these studies were based solely on a computational screening approach, without any experiments done to verify the calculations. Yu et al. used a combined experimental and computational study to probe for suitable quinone-based organic redox species.[21] Wedege et al. studied 33 compounds experimentally to investigate the influence of the side group position and number on redox potential and solubility.[22] Nevertheless, some aspects must still be discussed more precisely.

In this paper, based on the theory proposed by Palmer et al., who determined the intrinsic aqueous solubility of crystalline drug-like molecules by using first principles calculation, it is found that -OH groups could greatly improve the solubility.[23,24] In addition, it is suggested that 1,8-dihydroxyanthraquinone (1,8-DHAQ) may be a promising candidate for RFB based on the calculation of reduction potential. By rotating disk electrode measurements, it is found that the diffusion rate of 1,8-DHAQ is $4.97 \times 10^{-6} \text{ cm}^2 \text{ s}^{-1}$ and that the reaction speed is $2.2 \times 10^{-3} \text{ cm s}^{-1}$ (the corresponding parameter for $\text{VO}_2^+/\text{VO}^{2+}$ is $1 \sim 3 \times 10^{-6} \text{ cm s}^{-1}$), thus demonstrating excellent performance for RFB.

2. METHODS

2.1 Solubility Calculation

The intrinsic aqueous solubility of anthraquinone crystal is calculated according to the thermodynamic equilibrium, which is described as $\text{AQ}_s \rightleftharpoons \text{AQ}_{\text{aq}}$. AQ_s represents the undissolved crystalline form, and AQ_{aq} represents the neutral form in solution. The overall change in Gibbs free

energy is related to the intrinsic solubility (S) when a unified activity coefficient is supposed for the solute in solution, and this relationship is as follows:[25]

$$\Delta G_{\text{sol}} = \Delta G_{\text{sub}} + \Delta G_{\text{hyd}} = -RT \ln(SV_m) \quad (1-1)$$

where ΔG_{sol} is the solution energy, ΔG_{sub} is the sublimation energy, ΔG_{hyd} is the hydration energy, R is the molar gas constant, T is set to 298K, V_m is the molar volume of the crystal and S is the intrinsic solubility in units of mol L⁻¹.

Assuming a one atm standard state in the gas phase, the sublimation energy, $\Delta G_{\text{sub}}^{\circ}$, can be calculated by the Gibbs-Helmholtz equation

$$\Delta G_{\text{sub}}^{\circ} = \Delta H_{\text{sub}} - T\Delta S_{\text{sub}} \quad (1-2)$$

In this equation, the calculated lattice energy was used to estimate ΔH_{sub} , and ΔS_{sub} is the difference entropy under the ideal gas and crystal phase at 298K. In this manuscript, the calculated phonon models of the crystal were used to compute the entropy. Combined with the isothermal expansion formula of an ideal gas, ΔG_{sub} can be obtained using the following equation.

$$\Delta G_{\text{sub}} = \Delta G_{\text{sub}}^{\circ} - RT \ln\left(\frac{V_m p_0}{RT}\right) \quad (1-3)$$

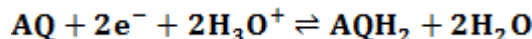
where p_0 is the standard atmosphere pressure (1 atm = 101.325 kPa). Combining the above two equations to eliminate V_m , the intrinsic solubility can be defined on the basis of $\Delta G_{\text{sub}}^{\circ}$ and ΔG_{hyd} .

$$S = \frac{p_0}{RT} \exp\left(\frac{\Delta G_{\text{sub}}^{\circ} + \Delta G_{\text{hyd}}}{-RT}\right) \quad (1-4)$$

ΔG_{hyd} can be obtained by implementing Gaussian software, M05-2X/6-31G* as the basic set and choosing SMD and IEFPCM models to compute the solvation effect. $\Delta G_{\text{sub}}^{\circ}$ was calculated using the SIESTA software, B-H (Berland-Hyldgaard) as the functional in the vdW-DF type.[26,27] Norm-conserving pseudopotentials and a triple zeta numerical plus polarization basis set were used in the calculations. These implicit-solvent protocols have been emphasized among the different types of prediction methods.[28]

2.2 Reduction Potential Calculation

As in previous work, the reduction of anthraquinone derivatives was treated as a single-step two-proton, two-electron process. The reduction potential of a species, AQ, can be computed by calculating the Gibbs energy of the following reaction:[29]



where AQ is the oxidation state of anthraquinone organic compound and AQH₂ is the reduction state. The reduction potential was calculated by the Nernst equation:

$$E_{\text{cal}} = -\frac{\Delta G'}{nF} \quad (2-1)$$

where $\Delta G'$ is the Gibbs free energy change, n = 2 is the number of electrons, and F is the Faraday constant.

$$\Delta G = G_{\text{AQH}_2} + 2G_{\text{H}_2\text{O}} - G_{\text{AQ}} - 2G_{\text{H}_3\text{O}^+} \quad (2-2)$$

Gibbs energy for every material can be calculated by using equation (2-3), and $G_{\text{ele}} + G_{\text{solv}}$ can be computed by using the SMD implicit solvent model with water as the solvent. The G_{freq} can be computed by the molecular frequency.

$$G = G_{\text{ele}} + G_{\text{freq}} + G_{\text{solv}} \quad (2-3)$$

Typically, one should subtract the equilibrium constant of water, which is equal to 55.5 mol/L, from the change in Gibbs free energy. Thus, the relationship between $\Delta G'$ and ΔG is given by equation (2-4).

$$\Delta G' = \Delta G - 2RT \ln[\text{H}_2\text{O}] \quad (2-4)$$

Combining equations (2-1) and (2-4) to eliminate $\Delta G'$, the calculated reduction potential E_{cal} can be obtained by equation (2-5).

$$E_{\text{cal}} = -\frac{\Delta G}{nF} + \frac{8RT}{nF} \quad (2-5)$$

where ΔG is given in units of eV, R is the molar gas constant, and T is set to 298K.

All electronic structure calculations were performed using the M05-2X/6-31G* as the basic set, as implemented in Gaussian software. The solvation effect can be calculated separately; IEFPCM and SMD model chemistry was used to calculate the electrostatic and non-electrostatic contributions, respectively.[30]

2.3 Electrochemical Measurements

In the experiments using a rotating disk electrode (RDE), 1 M KOH was used as a supporting electrolyte for the electrolyte solution, and 1 mM 1,8-DHAQ was used as the test sample. Oxygen was removed from the solution by purging with nitrogen for more than 30 minutes. For the RDE setup, a glassy carbon electrode of 3 mm in diameter, a Pt wire electrode and a Hg/HgO/KOH electrode were used as the working electrode, counter electrode and reference electrode, respectively. The glassy carbon electrode was polished to a mirror surface using 0.05 μm aluminium powder and then washed with ultrasonic and deionized water in turn before each test run. The standard hydrogen electrode (SHE) scale was preferred, and the electrode potentials were converted into it using the transformation equation $E(\text{SHE}) = E(\text{Hg/HgO/KOH}) + 0.098 \text{ V}$. For cyclic voltammetry, Ag/AgCl/3 M KCl electrode was used as the reference electrode, with a transformation formula $E(\text{SHE}) = E(\text{Ag/AgCl/KCl}) + 0.203 \text{ V}$.

3. RESULTS AND DISCUSSION

3.1 Solubility

Effective prediction of the probable solubility of organic compounds is very important in RFB technology, because it has a great impact on battery performance. An approach proposed by Palmer et al. that calculates the intrinsic aqueous solubility of crystalline drug-like molecules can be used to accurately investigate the solubility of organic species for RFBs. According to the previous report, 9,10-anthraquinone (9,10-AQ) was found to be most suitable for use in the anolyte on the negative side of RFBs.[18] Based on this same approach, we computed the solubility of three different 9,10-anthraquinone derivatives. Imitating a previous report, the schematic diagram of the calculation process is shown in Figure 1.[31]

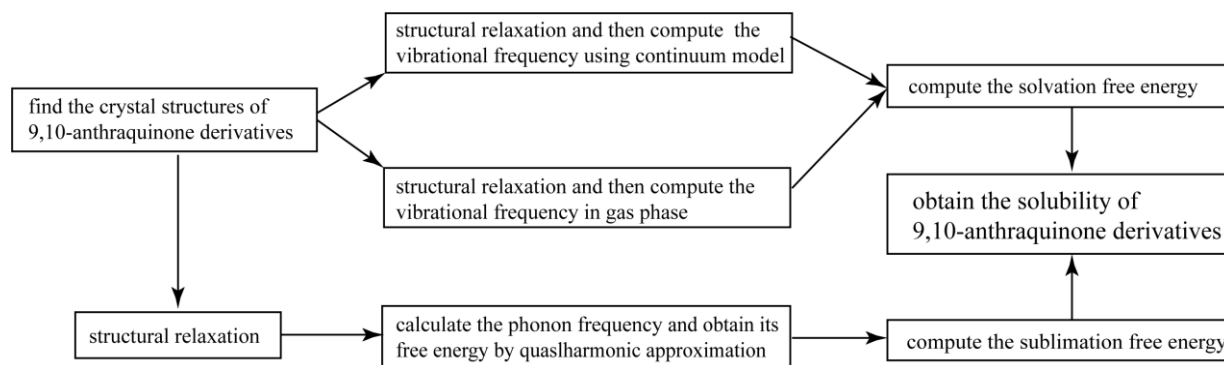


Figure 1. Scheme of the computational process for 9,10-anthraquinone derivatives' solubility.

As mentioned above, this study is, to the best of our knowledge, the first use of this method to predict the solubility of 9,10-anthraquinone derivatives. Use of the solvation energy to compute the solubility can result in some errors, especially for organic compounds for RFBs, because anthraquinone derivatives always have quite poor solubility. The calculation process is clear in the diagram, and we investigate the solubility of Benzamide (BZAMID02). The relaxed chemical structure is shown in Figure S1, and the relevant results obtained from calculations are shown in Table S1. Comparison of the experimental value and the calculated value for the solubility gives a bias of less than 1.7%. [23] Three different 9,10-anthraquinone derivatives, with three different substituent groups, namely, -OH, -SH and $-\text{NH}_2$, were discussed in this paper because electron-donating groups can greatly reduce the reduction potential, as noted in previous reports. [17,18] Thus, we chose three typical anthraquinone derivatives, **DHANTQ02** (1,5-dihydroxyanthraquinone), with two -OH groups, **KAPNIZ** (1,5-disulfhydrylanthraquinone), with two -SH groups, and **BOSMUS** (1,5-diaminoanthraquinone), with two $-\text{NH}_2$ groups; their chemical structures are shown in Figure 2.

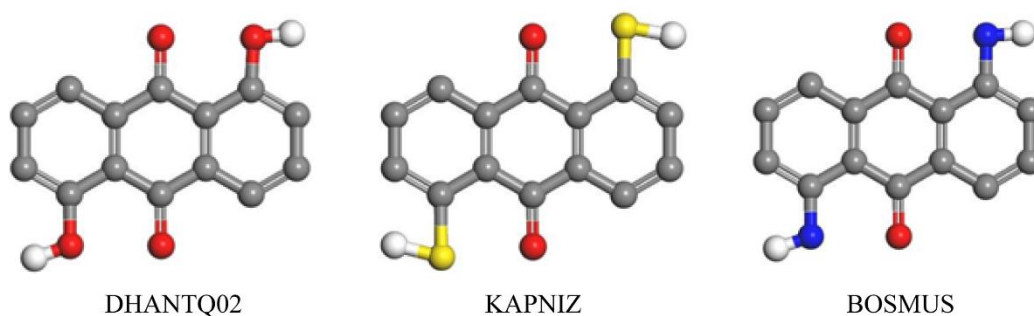


Figure 2. Chemical structures of **DHANTQ02** (1,5-dihydroxyanthraquinone), **KAPNIZ** (1,5-disulfhydrylanthraquinone) and **BOSMUS** (1,5-diaminoanthraquinone) represented by a ball-and-stick model. Grey, red, yellow blue and white balls indicate carbon, oxygen, sulfur, nitrogen and hydrogen atoms, respectively.

The Berland-Hyldgaard potential function was employed, and the density functional theory was used to model the structure relaxation process of crystal structure to an optical structure with the minimum energy. The optical structures obtained after structural relaxation are shown in Figure S2. The lattice parameters change slightly after relaxation, as shown in Table 1. The difference between

the lattice parameters is smaller than 5%, indicating that the structural relaxation process is realistic. For the derivatives, the lattice parameter a decreases, and b increases; further, the angles α and γ remain unchanged.

Table 1. Detailed lattice parameters of **DHANTQ02**, **KAPNIZ** and **BOSMUS** before and after structural relaxation; their structures are shown in Figure 2.

	before structural relaxation						after structural relaxation					
	a (Å)	b (Å)	c (Å)	α (°)	β (°)	γ (°)	a' (Å)	b' (Å)	c' (Å)	α' (°)	β' (°)	γ' (°)
DHANTQ02	6	5.3	15.8	90	93.7	90	5.8	5.5	15.6	90	95.8	90
KAPNIZ	3.9	10.4	13.7	90	93.6	90	3.7	10.6	13.9	90	90.3	90
BOSMUS	3.8	9.4	14.8	90	97.4	90	3.6	9.5	14.6	90	94.6	90

As is known, a known molecular crystal changing from a solid state into a gaseous state is an endothermic reaction. Therefore, in general, the sublimation free energy is positive, and the solvation energy is negative. The calculated solvation free energy and sublimation free energy are shown in Table 2. The solubility is determined by these two free energies. For clarity, the calculated S is shown as $\log S$, with a higher $\log S$ corresponding to a higher solubility. The results show that $\log S$ for **DHANTQ02** is calculated to be 0.765, which corresponds to an intrinsic solubility of approximately 5 mol L⁻¹. Although the electron-donating substituents -OH, -NH₂ and -SH have increasing reduction capabilities, the solubility of the 9,10-anthraquinone derivatives imparted by these substituent groups decreases in turn. Moreover, the solubility of -NH₂ and -SH is determined to be much smaller than that of -OH substitution at the same positions of 1 and 5.[32]

Table 2. Calculated $\Delta G_{\text{sub}}^{\text{cal}}$, $\Delta G_{\text{hyd}}^{\text{cal}}$, and $\log S^{\text{cal}}$ of **DHANTQ02**, **KAPNIZ** and **BOSMUS**, and their structures are shown in Figure 2.

	$\Delta G_{\text{sub}}^{\text{cal}}$ kJ/mol	$\Delta G_{\text{hyd}}^{\text{cal}}$ kJ/mol	$\log S^{\text{cal}}$
DHANTQ02	21.473	-33.756	0.765
KAPNIZ	152.705	-17.473	-25.092
BOSMUS	64.145	-45.907	-4.585

3.2 Reduction Potential

It is clear that there are small differences between the conventional calculations and ours. H^+ tends to form H_3O^+ when H^+ ions are surrounded by water. Considering this circumstance, we chose H_3O^+ to replace H^+ in the reduction reaction. To prove its accuracy, 11 quinone-based compounds were computed, and the results compared with previously reported values, as shown in Figure 3; the structures and calculated details of these 11 compounds are shown in Figure S2 and Table S2,

respectively. Clearly, the experimental values are well correlated with the calculated values, and this excellent linear relationship validates our calculations. The linear relationship between the calculated potential and that obtained from experiment has the form $y=0.78034x-3.66746$. The R^2 is approximately 0.99, which is very close to 1. Compared with previous reports, our calculations are more accurate and show a higher correlation.

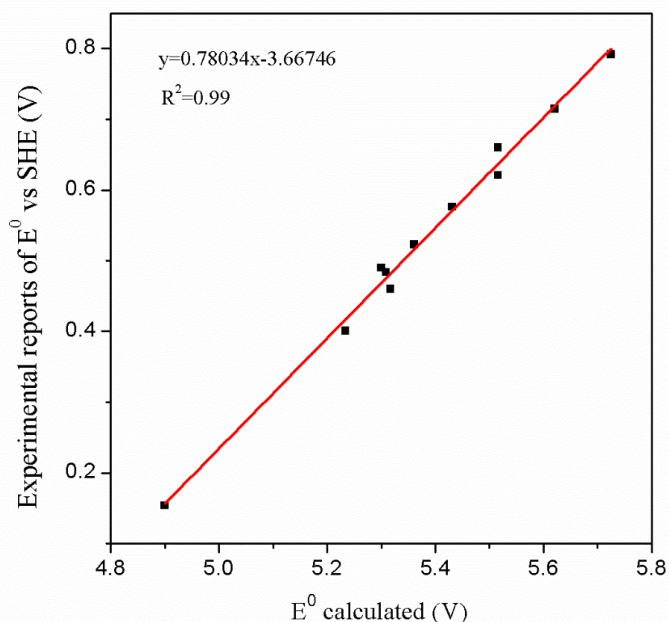


Figure 3. A straight line fit to calculated reduction potentials (vs SHE) versus experimental values.

Several reports have noted that the position of the side groups can have a significant impact on the electrochemical behaviour. For 9,10-anthraquinone derivatives, various substitution positions have been investigated in detail by experiments, which lead to the conclusion that the different substituting positions play a greater role than does the number of substitutions.[22,33] Three 9,10-anthraquinone derivatives were chosen to calculate the reduction potential based on the above parameters: **1,5-DHAQ** (1,5-dihydroxyanthraquinone), **1,8-DHAQ** (1,8-dihydroxyanthraquinone) and **2,6-DHAQ** (2,6-dihydroxyanthraquinone); their structures are shown in Figure 4.

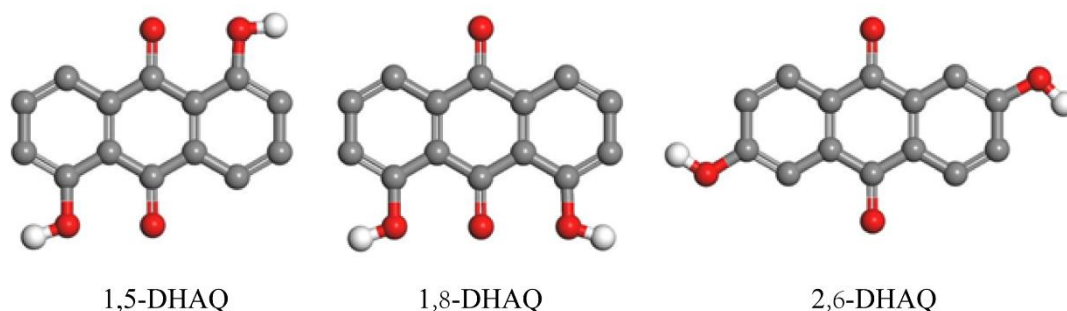
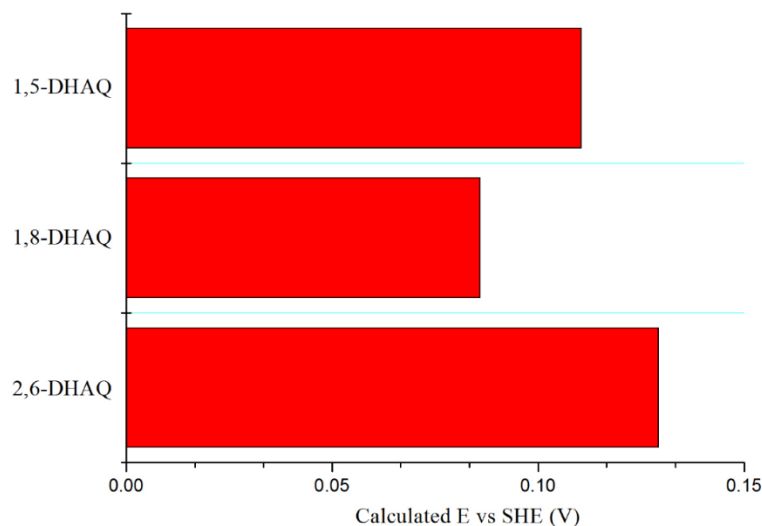


Figure 4. Structures of **1,5-DHAQ** (1,5-dihydroxyanthraquinone), **1,8-DHAQ** (1,8-dihydroxyanthraquinone) and **2,6-DHAQ** (2,6-dihydroxyanthraquinone). Grey, red and white balls indicate carbon, oxygen, and hydrogen atoms, respectively.

Table 3. Detailed calculated results of 1,5-DHAQ, 1,8-DHAQ and 2,6-DHAQ.

	G_{AQ}	G_{AQH_2}	G_{H_2O}	$G_{H_3O^+}$	ΔG	ΔG (eV)
1,5-DHAQ	-839.018	-840.179	-76.404	-76.811	-0.348	-9.476
1,8-DHAQ	-839.017	-840.176	-76.404	-76.811	-0.346	-9.413
2,6-DHAQ	-839.014	-840.177	-76.404	-76.811	-0.350	-9.524

**Figure 5.** Calculated reduction potential (vs SHE) of 1,5-DHAQ, 1,8-DHAQ and 2,6-DHAQ.

The calculation details are shown in Table 3, and the reduction potentials are shown in Figure 5. It can be speculated from previous research that $-OH$ can form hydrogen bonds with each other and thereby affect the calculated Gibbs free energy due to the solvation effect. Thus, $-OH$ substitution groups can decrease the reduction potential, with the extent of the decrease also related to the substituent position. Different substituent positions on the 9,10-anthraquinone derivatives have only a small influence on the reduction potential. The change, ΔE , is determined to be smaller than 30 mV. All of the calculated reduction potentials are above 0 V, with 2,6-DHAQ having the highest reduction potential of approximately 0.13 V. 1,8-DHAQ shows the lowest reduction potential of 0.08 V, which indicates that it can be considered the most suitable material for RFBs. Compared with the other two 9,10-anthraquinone derivatives, the positions of the $-OH$ substitutions in 2,6-DHAQ are the farthest apart; thus, its reduction potential is the highest, consistent with a previous report.[17]

3.3 Electrochemical Performance

Much research has been done to search for possible redox materials for RFBs as well as various ways to modify the organic compounds with electron-donating or electron-withdrawing groups. However, previous studies have tended to give a general conclusion without any further validation.[17,20,34] In this paper, electrochemical measurements were used to validate 1,8-DHAQ as a promising candidate for RFBs. Cyclic voltammetry data for 1,8-DHAQ recorded on a glassy carbon electrode are shown in Figure 6, which also shows the oxidation and reduction processes for the

material. Compared with previous reports, the sample shows similar redox performance and excellent reversibility, indicating that it is suitable for use as the negative material for RFBs.[33,35] Moreover, the reduction and oxidation peaks are at -577 mV and -615 mV, respectively. The peak separation of 38 mV is close to the value of 59 mV/n (n stands for the transferred electrons in reaction), which is equal to the oxidation potential subtracted from the reduction potential.[36] As noted previously, the reduction of 1,8-DHAQ is considered as a two-electron process. It is well known that an excellent indicator of a multielectrode quasi-reversible process is a peak separation value no greater than 59 mV.[37] Therefore, 1,8-DHAQ meets the requirement of loop performance for a flow cell.

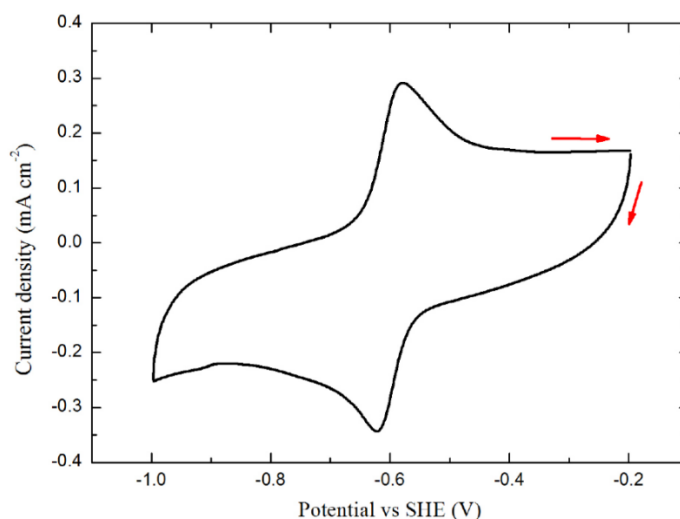


Figure 6. Cyclic voltammogram of 1,8-DHAQ on a glassy carbon electrode (scan rate is 25 mV s⁻¹).

Rotating disk electrode measurements were used to characterize the diffusion and electron transfer properties of 1,8-DHAQ, and the results are shown in Figure 7. According to the analysis of the Levich plot, the diffusion coefficient was obtained as

$$i_l = 0.620nFAD^{2/3}\nu^{-1/6}\omega^{1/2}C^b \quad (3-1)$$

where i_l is the mass-transport-limited current density, F is the Faraday constant (96548 C mol⁻¹), A is the electrode area (0.2475 cm²), D is the diffusion coefficient, n is the molar electron number, ν is the kinematic viscosity (0.01 cm²s⁻¹), ω is the rotation rate in rad s⁻¹ and C^b is the 1,8-DHAQ bulk concentration (10⁻⁶ mol cm⁻³). The diffusion coefficient of 1,8-DHAQ was calculated to be 4.97×10^{-6} cm²s⁻¹, which is about twice as large as the previous report for redox flow batteries.[37] Next, the Koutecký-Levich plot for 1,8-DHAQ was derived from the RDE data, as shown in Figure 7c. From this plot, the relationship between current and overpotential can be determined by a fit to the simplified Butler-Volmer equation without any mass-transfer effects:

$$\eta = \frac{2.303RT}{\alpha nF} \log i_0 - \frac{2.303RT}{\alpha nF} \log i \quad (3-2)$$

where i is the measured current density, i_0 is the exchange current, η is the overpotential. The exchange current density i_0 was found using the fit to the data shown in Figure 7d. The rate constant can be obtained through the following equation:

$$k = \frac{i_0}{FAC_0} \tag{3-3}$$

After a series of calculations, the kinetic rate constant of 1,8-DHAQ was determined to be $2.2 \times 10^{-3} \text{ cm s}^{-1}$, which is much faster compared to that found for many other redox materials used in RFBs, especially conventional metal redox species.[38]

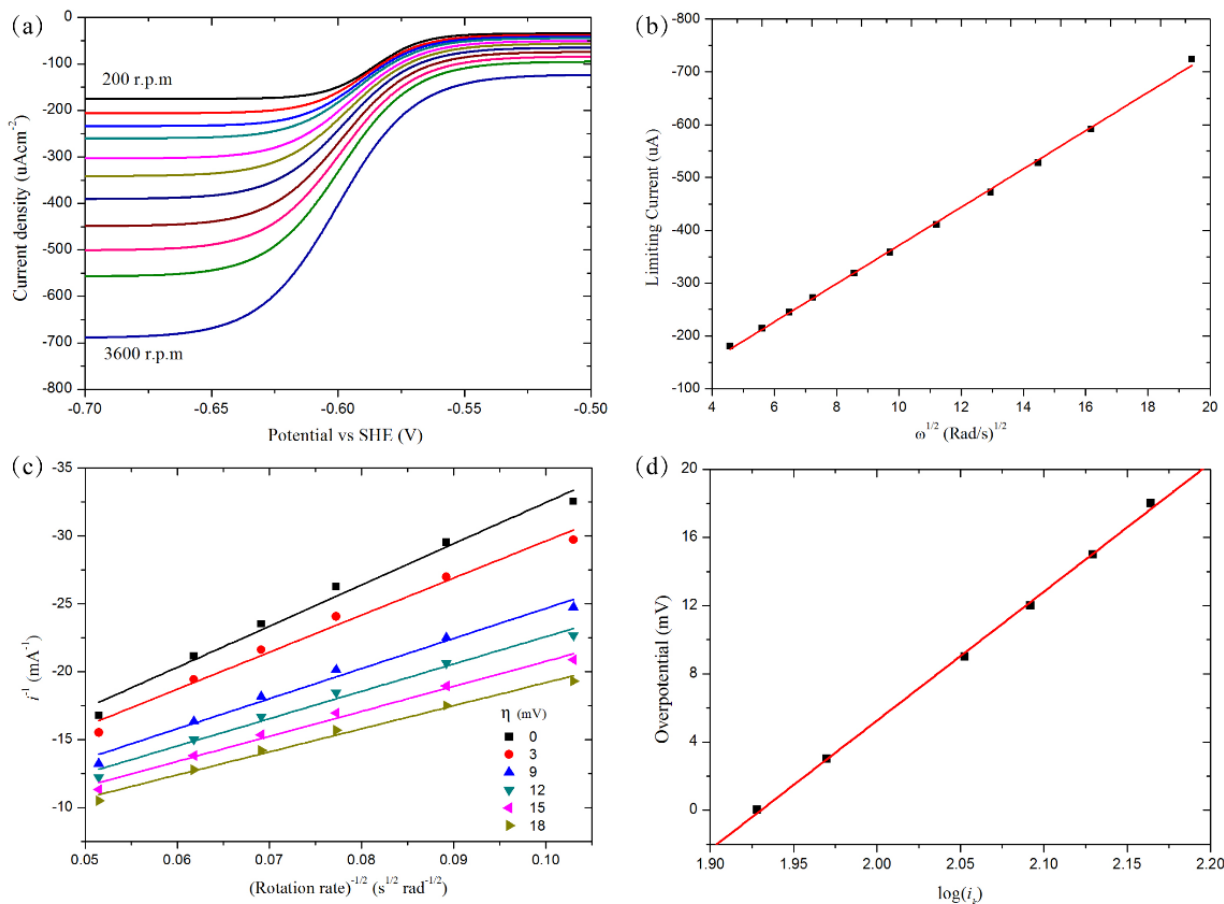


Figure 7. Electrochemical test results. (a) Rotating disk electrode measurements of 1,8-DHAQ at 11 rotation rates ranging from 200 r.p.m.(black) to 3000 r.p.m.(blue). (b) Levich plot showing the relationship between limiting current and rotation rate derived from Figure 7a. (c) Koutecký-Levich plot derived from Figure 7a at six different reduction overpotentials. (d) The curve fit to the Butler-Volmer equation derived from Figure 7c for 1,8-DHAQ.

4. CONCLUSION

This is a comparatively integral work on seeking suitable negative active materials for redox flow batteries. First, we calculated the solubility and reduction potential to find theoretically suitable materials, and we then examined the computational results by electrochemical measurements. According to the solubility calculation, we found that $-OH$ could greatly improve the solubility, with a theoretical solubility of approximately 5 mol/L, a theoretical reduction potential of approximately 0.1 V, and a diffusion coefficient and kinetic rate constant of $4.97 \times 10^{-6} \text{ cm}^2/\text{s}$ and $2.2 \times 10^{-3} \text{ cm/s}$

respectively, which is faster compared with those of many other redox materials used in RFBs. Combined with theoretical calculations, it is a quite efficient method for finding suitable materials and can increase the research speed to a great extent.

ACKNOWLEDGEMENT

This work was funded through Beijing Institute of Technology scientific cooperation project (3190012351701), the National Nature Science Foundation of China (No. 20806008) and the National Nature Science Foundation of China (No. 21111120074).

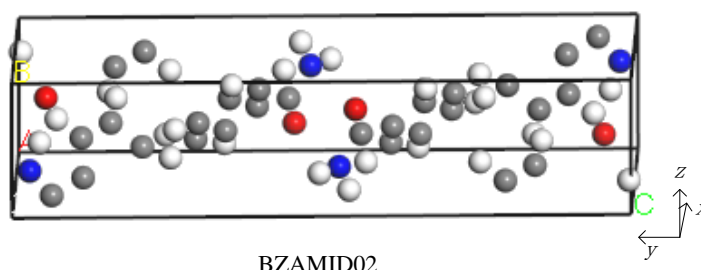


Figure S1. Optical structure of Benzamide after structural relaxation.

Table S1. Calculated and experimental values of ΔG_{sub} , ΔG_{hyd} and $\log S$ of **BZAMID02**.

	ΔG_{sub}^{cal}	ΔG_{hyd}^{cal}	$\log S^{cal}$	$\Delta G_{sub}^{exp a}$	$\Delta G_{hyd}^{exp a}$	$\log S^{exp a}$
	kJ/mol	kJ/mol	mol/L	kJ/mol	kJ/mol	mol/L
BZAMID02	41.497	-43.903	-0.966	-43.14	-45.64	-0.95

a derived from ref. 23.

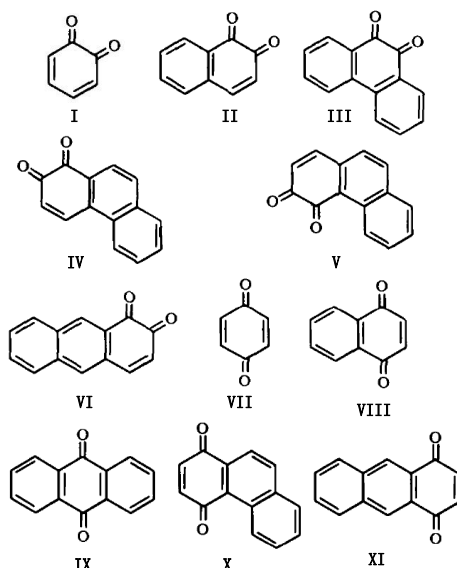
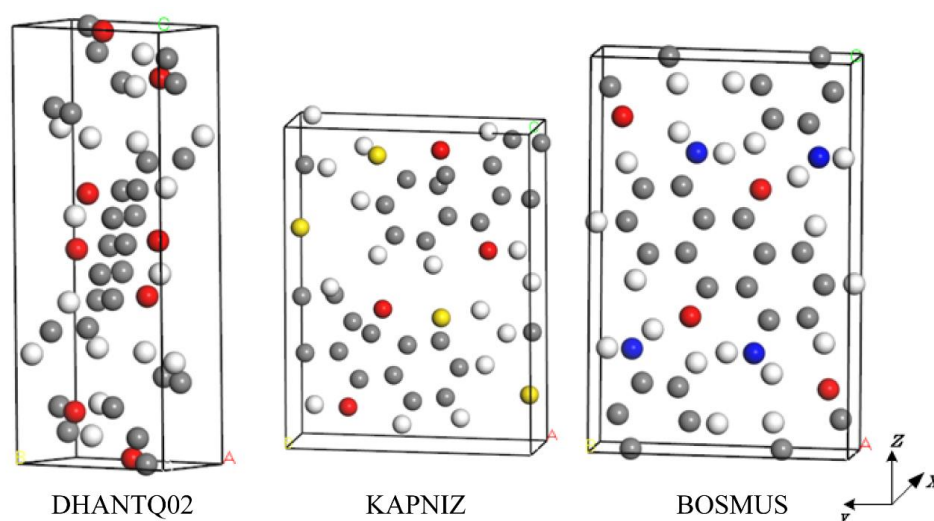


Figure S2. Eleven compounds of quinone derived from ref. 2.

Table S2. Calculated redox potential of quinone compounds from I to XI. The corresponding structures are shown in Figure S2.

	G_{AQ}	G_{AQH_2}	G_{H_2Q}	$G_{H_3O^+}$	ΔG	ΔG	E_{cal}	E_{exp}^b
	Hartree	Hartree	Hartree	Hartree	Hartree	eV	V	V
I	-381.346	-382.573	-76.404	-76.811	-0.413	-11.244	5.725	0.792
II	-534.959	-536.163	-76.404	-76.811	-0.392	-10.656	5.431	0.576
III	-688.561	-689.758	-76.404	-76.811	-0.383	-10.428	5.317	0.460
IV	-688.547	-689.758	-76.404	-76.811	-0.398	-10.826	5.516	0.660
V	-688.545	-689.756	-76.404	-76.811	-0.398	-10.826	5.516	0.621
VI	-688.552	-689.748	-76.404	-76.811	-0.382	-10.394	5.300	0.490
VII	-381.355	-382.573	-76.404	-76.811	-0.406	-11.035	5.621	0.715
VIII	-534.967	-536.163	-76.404	-76.811	-0.383	-10.411	5.309	0.484
IX	-688.578	-689.744	-76.404	-76.811	-0.353	-9.594	4.900	0.154
X	-688.560	-689.750	-76.404	-76.811	-0.377	-10.262	5.234	0.401
XI	-688.552	-689.752	-76.404	-76.811	-0.386	-10.516	5.361	0.523

b derived from ref. 39.

**Figure S3.** Optical structures of **DHANTQ02** (1,5-dihydroxyanthraquinone), **KAPNIZ** (1,5-disulphydrylanthraquinone) and **BOSMUS** (1,5-diaminoanthraquinone) after structural relaxation.

References

1. B. Dunn, H. Kamath and J.-M. Tarascon, *Science*, 334 (2011) 928.
2. Z. G. Yang, J. L. Zhang, M. C. W. Kintner-Meyer, X. C. Lu, D. W. Choi, J. P. Lemmon and J. Liu, *Chem. Rev.*, 111 (2011) 3577.
3. C. P. de Leon, A. Frias-Ferrer, J. Gonzalez-Garcia, D. A. Szanto and F. C. Walsh, *J. Power Sources*, 160 (2006) 716.
4. F. R. Brushett, J. T. Vaughey and A. N. Jansen, *Adv. Energy Mater.*, 2 (2012) 1390.
5. D. Chu, X. Li and S. Zhang, *Electrochim. Acta*, 190 (2016) 434.
6. P. Leung, X. H. Li, C. P. de Leon, L. Berlouis, C. T. J. Low and F. C. Walsh, *Rsc Adv.*, 2 (2012) 10125.
7. S. H. Oh, C. W. Lee, D. H. Chun, J. D. Jeon, J. Shim, K. H. Shin and J. H. Yang, *J. Mater. Chem. A*, 2 (2014) 19994.
8. S. Jeong, S. Kim and Y. Kwon, *Electrochim. Acta*, 114 (2013) 439.
9. Q. Huang and Q. Wang, *Chempluschem*, 80 (2015) 312.
10. M. Skyllas-Kazacos, M. H. Chakrabarti, S. A. Hajimolana, F. S. Mjalli and M. Saleem, *J. Electrochem. Soc.*, 158 (2011) R55.
11. G. L. Soloveichik, *Chem. Rev.*, 115 (2015) 11533.
12. J. Noack, N. Roznyatovskaya, T. Herr and P. Fischer, *Angew. Chem. Int. Edit.*, 54 (2015) 9775.
13. S. Kim, J. L. Yan, B. Schwenger, J. L. Zhang, L. Y. Li, J. Liu, Z. G. Yang and M. A. Hickner, *Electrochem. Commun.*, 12 (2010) 1650.
14. B. Yang, L. Hooper-Burkhardt, S. Krishnamoorthy, A. Murali, G. K. S. Prakash and S. R. Narayanan, *J. Electrochem. Soc.*, 163 (2016) A1442.
15. R. M. Darling, K. G. Gallagher, J. A. Kowalski, S. Ha and F. R. Brushett, *Energ. Environ. Sci.*, 7 (2014) 3459.
16. T. Janoschka, N. Martin, U. Martin, C. Friebe, S. Morgenstern, H. Hiller, M. D. Hager and U. S. Schubert, *Nature*, 527 (2015) 78.
17. Z. Wang, A. Li, L. Gou, J. Ren and G. Zhai, *Rsc Adv.*, 6 (2016) 89827.
18. S. Er, C. Suh, M. P. Marshak and A. Aspuru-Guzik, *Chem. Sci.*, 6 (2015) 885.
19. S. D. Pineda Flores, G. C. Martin-Noble, R. L. Phillips and J. Schrier, *J. Phys. Chem. C*, 119 (2015) 21800.
20. Y. Moon and Y.-K. Han, *Curr. Appl. Phys.*, 16 (2016) 939.
21. Y. Ding, Y. Li and G. Yu, *Chem*, 1 (2016) 790.
22. K. Wedege, E. Drazevic, D. Konya and A. Bentien, *Sci. Rep.*, 6 (2016) 39101.
23. D. S. Palmer, J. L. McDonagh, J. B. Mitchell, T. van Mourik and M. V. Fedorov, *J. Chem. theory Comput.*, 8 (2012) 3322.
24. E. L. Ratkova, D. S. Palmer and M. V. Fedorov, *Chem. Rev.*, 115 (2015) 6312.
25. J. L. McDonagh, N. Nath, L. De Ferrari, T. van Mourik and J. B. Mitchell, *J. Chem. Inf. Model.*, 54 (2014) 844.
26. T. J. Hou, K. Xia, W. Zhang and X.J. Xu, *J. Chem. Inf. Comput. Sci.*, 44 (2004) 266.
27. K. Berland and P. Hyldgaard, *Phys. Rev. B*, 89 (2014).
28. A.V. Marenich, J. Ho, M.L. Coote, C.J. Cramer and D.G. Truhlar, *Phys. Chem. Chem. Phys.*, 16 (2014) 15068.
29. M. Quan, D. Sanchez, M. F. Wasylkiw and D. K. Smith, *J. Am. Chem. Soc.*, 129 (2007) 12847.
30. S. Miertus, E. Scrocco, J. Tomasi, *Chem. Phys.*, 55 (1981) 117.
31. C. Schütter, T. Husch, M. Korth and A. Balducci, *J. Phys. Chem. C*, 119 (2015) 13413.
32. R. Qu, H. Liu, M. Feng, X. Yang and Z. Wang, *J. Chem. Eng. Data*, 57 (2012) 2442.
33. M. R. Gerhardt, L. Tong, R. Gómez-Bombarelli, Q. Chen, M. P. Marshak, C. J. Galvin, A. Aspuru-Guzik, R. G. Gordon and M. J. Aziz, *Adv. Energy Mater.*, 7 (2017) 1601488.
34. J. E. Bachman, L. A. Curtiss and R. S. Assary, *J. Phys. Chem. A*, 118 (2014) 8852.

35. Q. C. Kaixiang Lin, *Science*, 349 (2015) 1529.
36. B. Huskinson, M. P. Marshak, C. Suh, S. Er, M. R. Gerhardt, C. J. Galvin, X. Chen, A. Aspuru-Guzik, R. G. Gordon and M. J. Aziz, *Nature*, 505 (2014) 195.
37. S. Zhang, X. Li and D. Chu, *Electrochim. Acta*, 190 (2016) 737.
38. A. Z. Weber, M. M. Mench, J. P. Meyers, P. N. Ross, J. T. Gostick and Q. H. Liu, *J. Appl. Electrochem.*, 41 (2011) 1137.
39. K. V. Balakin, N. P. Savchuk and I. V. Tetko, *Curr. Med. Chem.*, 13 (2006) 223.

© 2017 The Authors. Published by ESG (www.electrochemsci.org). This article is an open access article distributed under the terms and conditions of the Creative Commons Attribution license (<http://creativecommons.org/licenses/by/4.0/>).